Pressure-induced changes of the structure and properties of monoclinic α-chalcocite Cu_2S

D. Zimmer,[1,*] J. Ruiz-Fuertes,[2,3] W. Morgenroth,[1] A. Friedrich,[4] L. Bayarjargal,[1] E. Haussühl,[1]
D. Santamaría-Pérez,[3] S. Frischkorn,[1] V. Milman,[5] and B. Winkler[1]

[1]*Institute of Geosciences, Goethe-University Frankfurt, 60438 Frankfurt am Main, Germany*
[2]*DCITIMAC, Universidad de Cantabria, 39005 Santander, Spain*
[3]*Departament de Física Aplicada-ICMUV, Universitat de València, 46100 Burjassot, Spain*
[4]*Institut für Anorganische Chemie, Julius-Maximilians-Universität Würzburg, 97074 Würzburg, Germany*
[5]*Dassault Systèmes BIOVIA, CB4 0WN Cambridge, United Kingdom*

(Received 16 February 2018; published 13 April 2018)

The high-pressure behavior of monoclinic ($P2_1/c$) α-chalcocite, Cu_2S, was investigated at ambient temperature by single-crystal x-ray diffraction, electrical resistance measurements, and optical absorption spectroscopy up to 16 GPa. The experiments were complemented by density-functional-theory-based calculations. Single-crystal x-ray diffraction data show that monoclinic α-chalcocite undergoes two pressure-induced first-order phase transitions at ∼3.1 and ∼7.1 GPa. The crystal structure of the first high-pressure polymorph, HP1, was solved and refined in space group $P2_1/c$ with $a = 10.312(4)$ Å, $b = 6.737(3)$ Å, $c = 7.305(1)$ Å, and $\beta = 100.17(2)^\circ$ at 6.2(3) GPa. The crystal structure of the second high-pressure polymorph, HP2, was solved and refined in space group $P2_1/c$ with $a = 6.731(4)$ Å, $b = 6.689(2)$ Å, $c = 6.967(8)$ Å, and $\beta = 93.18(3)^\circ$ at 7.9(4) GPa. Electrical resistance measurements upon compression and optical absorption experiments upon decompression show that the structural changes in α-chalcocite are accompanied by changes of the electrical and optical properties. Upon pressure release, the band gap E_g of α-chalcocite (1.24 eV at ambient conditions) widens across the first structural phase transition, going from 1.24 eV at 2.2 GPa (α-chalcocite) to 1.35 eV at 2.6 GPa (HP1), and closes significantly across the second phase transition, going from 1.32 eV at 4.4 GPa (HP1) to 0.87 eV at 4.9 GPa (HP2). The electrical resistance shows similar behavior: its highest value is for the first high-pressure polymorph (HP1), and its lowest value is for the second high-pressure polymorph (HP2) of α-chalcocite. These results are interpreted on the basis of calculated electronic band structures.

DOI: 10.1103/PhysRevB.97.134111

I. INTRODUCTION

Monoclinic α-chalcocite [1], Cu_2S, is one of the dominant mineral phases in copper ores and has been investigated extensively for the last 100 years due to its outstanding physical properties, such as ion conductivity at elevated temperatures [2], fast switchable phase transitions [3], and semiconductivity [2]. Its optical band gap of about 1.2 eV [4–6] makes α-chalcocite, in principle, suitable for applications as an absorber material in solar cells. The ubiquity of copper sulfide together with its low cost and nontoxicity made Cu_2S-based solar cells one of the most intensively studied systems [7]. Unfortunately, the limited phase stability of α-chalcocite has prevented Cu_2S-based solar cells from being produced commercially on a large industrial scale [8,9]. In the recent course of the rapidly growing research on nanocrystalline materials copper sulfides have attracted renewed interest [10]. Nanoparticles of tetragonal copper sulfide [11], Cu_2S, a high-pressure, high-temperature polymorph of monoclinic α-chalcocite, were found to exhibit an extended phase stability after doping with iron [12]. According to Machani *et al.* [12], nanoparticles of tetragonal copper sulfide exhibit optical properties similar to those of monoclinic α-chalcocite, drawing attention to nonambient phases of copper sulfides in general. However, a recently described temperature-induced phase transition of tetragonal copper sulfide at moderately low temperatures [13] might be disadvantageous for applications in solar cells.

Nevertheless, it now is intriguing to further investigate the high-pressure behavior of Cu_2S, as pressure-induced phase transitions have already been reported, and hence, it is worthwhile to explore whether or not high-pressure phases may be suitable for energy-conversion applications.

The first attempts to describe the crystal structure of α-chalcocite at ambient conditions were published by Buerger and Buerger [14], who employed an orthorhombic unit cell with $a = 11.92$ Å, $b = 27.84$ Å, and $c = 13.44$ Å. Later, this structural model was replaced by a monoclinic model (space group: $P2_1/c$) by Evans [1] which was further refined again by Evans [15] with $a = 15.246(4)$ Å, $b = 11.884(2)$ Å, $c = 13.494(3)$ Å, and $\beta = 116.35(1)^\circ$. According to the monoclinic model the structure of α-chalcocite is based on a hexagonal close packing of sulfur with copper dominantly in trigonal planar and distorted tetrahedral coordination, as shown in Fig. 1. Early high-pressure, high-temperature studies of Cu_2S published by Skinner [16] and Seifert [17] showed that at elevated temperatures and pressures between 0.5 GPa/373 K and 9 GPa/737 K tetragonal copper sulfide, Cu_2S, is the only polymorph that can be recovered metastably at ambient conditions. The first *in situ* high-pressure x-ray diffraction experiments at ambient temperature on Cu_2S were performed

*zimmer@kristall.uni-frankfurt.de

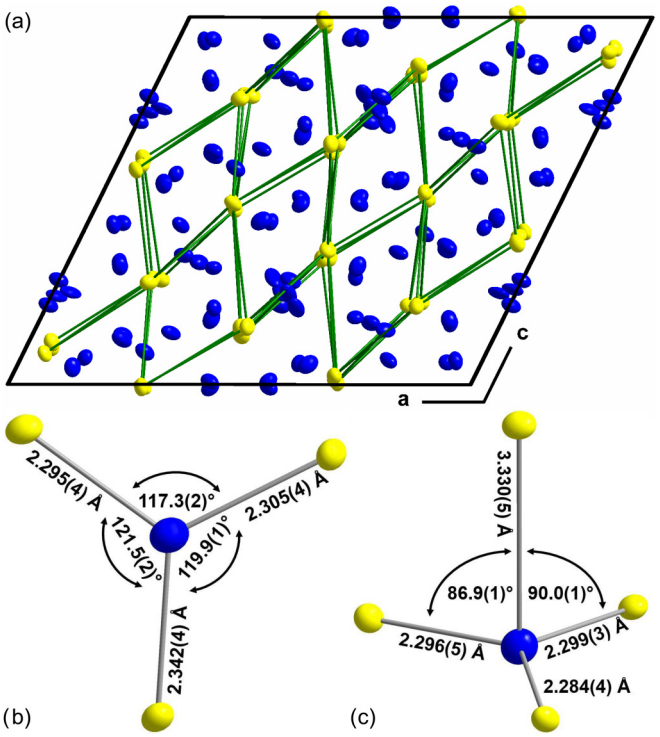

FIG. 1. Structural properties of α-chalcocite [$a = 15.1882(6)$ Å, $b = 11.8511(4)$ Å, $c = 13.465(2)$ Å, and $\beta = 116.263(5)^\circ$] at ambient conditions evaluated by single-crystal x-ray diffraction [21] based on the structural model by Evans [15]. (a) View along the crystallographic axis b. Blue: copper; yellow: sulfur; green lines: indication of the distorted hexagonal close packing of sulfur. (b) Trigonal planar coordination of copper in α-chalcocite: typical values for Cu-S distances and angles. (c) Fourfold coordination of copper in α-chalcocite showing a distorted tetrahedral character: typical values for Cu-S distances and angles.

by Hinze and Neuhaus [18] using a diamond "squeezer," in which a very large pressure gradient across the sample results from the almost solely uniaxial compression. The authors found three pressure-induced phase transitions up to 10 GPa accompanied by a disproportion of Cu_2S into CuS_2 and copper. Further *in situ* high-pressure powder x-ray diffraction experiments at ambient temperature and quasihydrostatic conditions were carried out by Wang *et al.* [19] and Santamaría-Pérez *et al.* [20] in diamond-anvil cells up to about 20 and 30 GPa, respectively. Both studies show that monoclinic α-chalcocite, Cu_2S, undergoes two reversible pressure-induced phase transitions up to 10 GPa, transforming into high-pressure polymorphs HP1 and HP2, respectively. For the two new polymorphs Santamaría-Pérez *et al.* [20] and Wang *et al.* [19] proposed different unit cells but were not able to solve the structures from the powder data (see Supplemental Material [21] for a brief comparison of the unit cells). In the present high-pressure study we employed single crystals of monoclinic α-chalcocite instead of powder samples. This allowed us to solve the crystal structures.

II. EXPERIMENTAL DETAILS

X-ray diffraction experiments and optical absorption measurements on α-chalcocite, Cu_2S, were performed on natural

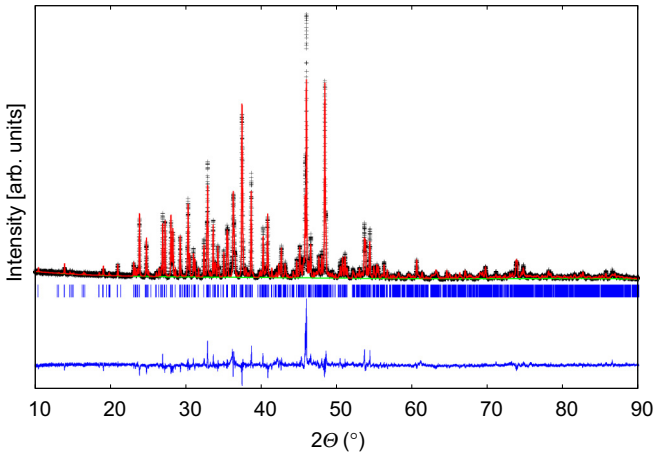

FIG. 2. Powder x-ray diffraction pattern of α-chalcocite, Cu_2S, at ambient conditions and Rietveld refinement based on structural data published by Evans [15] ($\lambda = 1.5406$ Å). Black crosses: measured data; red line: simulated pattern; green line: background; blue line: residuals; blue tick marks: calculated reflection positions.

single crystals ($\sim 50 \times 50 \times 10\,\mu m^3$) from Wolfach (Germany). The chemical composition of the natural copper sulfide samples was determined by energy-dispersive x-ray spectroscopy using a scanning electron microscope (Phenom ProX, Phenom-World), equipped with an energy-dispersive detector. The chemical analysis of the natural samples shows that there is no chemical impurity in the natural single crystals [21] above our experimental sensitivity of about 0.5 wt %. In order to perform electrical resistance measurements at high pressure we also produced α-chalcocite in powder form by a synthesis from the elements (copper: 99.99%, ChemPUR, Karlsruhe; sulfur: 99.99%, Sigma-Aldrich, Missouri) in evacuated silica tubes at 900 K. The product of the synthesis in the silica tubes consisted of a homogeneous opaque powder. The powder samples were characterized by powder x-ray diffraction using an X-PertPro diffractometer equipped with a linear position-sensitive detector from PANalytical (PIXcel^{3D}) and a Johannson monochromator (Ge 111) using Cu $K\alpha_1$ radiation. The powder was applied on a silicon single-crystal plate. Data were collected with a step width of 0.003° between 10° and 90° and a total measurement time of about 14 h. The Rietveld refinements [22] were performed by employing GSAS [23] with the EXPGUI [24] package. The high quality of the powder x-ray diffraction pattern of the product at ambient conditions allowed a successful Rietveld refinement based on structural data for α-chalcocite published by Evans [15], as shown in Fig. 2 (see Supplemental Material [21] for the details of the refinement).

High-pressure experiments were carried out in Boehler-Almax-type diamond-anvil cells [25] using neon or a mixture of methanol and ethanol (4:1) as a quasihydrostatic pressure-transmitting medium. The pressure was determined by the shift of the ruby luminescence based on the calibration established by Mao *et al.* [26].

Single-crystal x-ray diffraction at ambient conditions was performed using an Xcalibur3 four-circle diffractometer from Rigaku (formerly Oxford Diffraction) equipped with graphite-

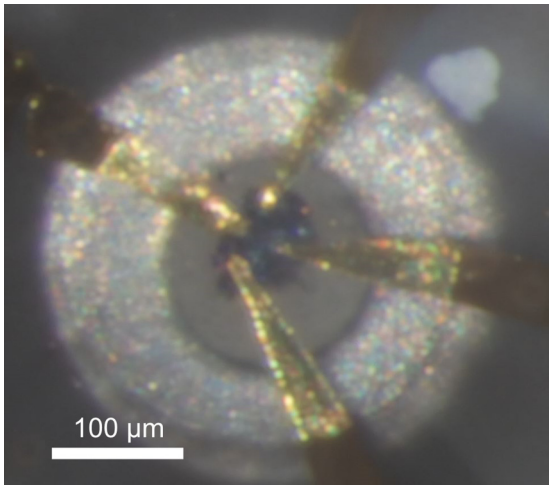

FIG. 3. Experimental setup for four-wire electrical resistance measurements in a diamond-anvil cell. Four gold wires are connected to an α-chalcocite sample embedded in a mixture of epoxy resin and aluminium oxide surrounded by a tungsten gasket.

monochromatized Mo $K\alpha$ radiation and a charge-coupled-device camera (Sapphire3). The samples were mounted on the goniometer head at a distance of 42 mm to the detector. Single-crystal synchrotron x-ray diffraction was performed as a function of pressure in diamond-anvil cells at the Extreme Conditions Beamline P02.2 [27] at PETRA III, DESY, Hamburg, Germany, with a wavelength of 0.2904 Å, a spot size of $\sim 8 \times 4\ \mu m^2$, and a distance of ~400 mm between the sample and the detector. The data were collected using a PerkinElmer XRD 1621 flat-panel detector while rotating the sample by 0.5° in ω. Indexing, data reduction, and empirical absorption correction were performed using the CRYSALIS^{PRO} software from Rigaku (formerly Agilent) [28]. Structure solutions and structural refinements were performed using SUPERFLIP [29] and JANA2006 [30], respectively.

The electrical properties of α-chalcocite, Cu_2S, were determined as a function of pressure up to ~10 GPa by four-wire resistance measurements in a diamond-anvil cell. Four gold wires were used to establish contact between the multimeter (DMM7510, Keithley) and α-chalcocite, as shown in Fig. 3. The wires and the sample were insulated from the tungsten gasket by a mixture of epoxy resin and aluminum oxide, which also acted as the pressure-transmitting medium. At each pressure step 1000 resistance measurements were performed. Possible errors due to thermoelectric effects were avoided by alternating the direction of the excitation current.

Optical absorption measurements were performed in a custom-built confocal system equipped with two Cassegrain objectives and a halogen lamp. The spectrometers used were a near-infrared (NIR) StellarNet equipped with an InGaAs

TABLE I. Parameters and results of single-crystal x-ray diffraction data collections, data reductions, and crystal structure refinements based on F. In obs/all, obs = $I > 3\sigma$, $w = 1/[\sigma^2(F) + 0.0001(F)^2]$.

	Phase		
	α-chalcocite	HP1	HP2
	Crystal data		
Chemical formula	Cu_2S	Cu_2S	Cu_2S
Cell parameters			
a (Å)	15.1882(6)	10.312(4)	6.731(4)
b (Å)	11.8511(4)	6.737(3)	6.689(2)
c (Å)	13.465(5)	7.305(1)	6.967(8)
β (°)	116.263(8)	100.17(2)	93.18(3)
V (Å^3)	2173.5(1)	499.5(1)	313.2(1)
Z	48	12	8
Space group	$P2_1/c$	$P2_1/c$	$P2_1/c$
ρ (g/cm^3)	5.8365(1)	6.2370(1)	6.7825(1)
	Data collection		
Temperature (K)	293(5)	293(5)	293(5)
Pressure (GPa)	0.0001	6.2(3)	7.9(4)
λ (Å)	0.71073	0.2904	0.2904
$\mathrm{Sin}\theta_{max}/\lambda$ (Å^{-1})	0.6921	1.0746	1.0694
Reflection range	$-20 \leqslant h \leqslant 19$	$-20 \leqslant h \leqslant 20$	$-13 \leqslant h \leqslant 13$
	$-16 \leqslant k \leqslant 16$	$-11 \leqslant k \leqslant 9$	$-12 \leqslant k \leqslant 13$
	$-18 \leqslant l \leqslant 18$	$-15 \leqslant l \leqslant 15$	$-6 \leqslant l \leqslant 4$
No. of reflections obs/all	12632/33203	3027/3635	1415/1720
Unique reflections obs/all	2724/5292	1754/1974	719/877
R_{int}, obs/all	0.050/0.087	0.023/0.027	0.031/0.031
	Refinement		
No. of parameters	333	91	50
R, obs/all	0.040/0.1212	0.047/0.051	0.080/0.091
wR, obs/all	0.034/0.048	0.065/0.066	0.102/0.103

detector for the NIR part and an OCEAN HR4000 for the visible-NIR region.

III. COMPUTATIONAL DETAILS

First-principles calculations were carried out within the framework of density-functional theory (DFT) [31] using the generalized gradient approximation Perdew-Burke-Ernzerhof [32] functional and the pseudopotential method using the CASTEP [33] simulation package. On-the-fly ultrasoft pseudopotentials from the CASTEP database were employed in conjunction with plane waves up to a kinetic-energy cutoff of 450 eV. A Monkhorst-Pack [34] grid was used for Brillouin-zone integrations with a distance of <0.025 Å^{-1} between grid points. Convergence criteria included an energy change of $<5 \times 10^{-7}$ eV/atom for self-consistent field cycles, a maximal force of <0.01 eV/Å, and a maximal component of the stress tensor <0.02 GPa.

IV. RESULTS AND DISCUSSION

A. Single-crystal x-ray diffraction

At ambient conditions the structure of α-chalcocite was solved and refined in space group $P2_1/c$ based on single-crystal x-ray diffraction data (Fig. 1) with $a = 15.1882(6)$ Å, $b = 11.8511(4)$ Å, $c = 13.465(2)$ Å, and $\beta = 116.263(5)^\circ$, in accordance with the structural model published by Evans [15]. The anisotropic thermal displacement parameters were refined successfully for all 38 atomic sites (Table I and Supplemental Material [21]). Due to unusually high values for the anisotropic displacement parameters in one direction of two copper positions (Cu23, Cu24) disorder was assumed, and therefore, these copper sites were split (Cu23, Cu23′, Cu24, Cu24′). The site occupation factors and the anisotropic thermal displacement parameters for these four copper sites were refined successfully [21]. The unusually high values of the displacement parameters at these two sites were also mentioned by Evans [15], but according to the author neither a splitting of the atomic sites nor a refinement in a lower-symmetry space group led to a physically acceptable model. Structural solutions and refinements in space groups with lower symmetry (Pc, $P2_1$) were unsuccessful in the scope of the present work as well.

The structure of α-chalcocite is based on a distorted hexagonal close packing of sulfur with 26 symmetrically independent Wyckoff positions (4e) for copper and 12 symmetrically independent Wyckoff positions (4e) for sulfur (Fig. 1). Four of the copper positions have a site occupation factor close to 0.5 and belong to the small disordered part of the structure. In a single unit cell 92 of the 96 copper atoms are coordinated trigonal planar by three sulfur atoms with Cu-S distances of about 2.3 Å. Sixty of those copper atoms are coordinated by a fourth sulfur atom at a distance >3.0 Å towards a highly distorted tetrahedral coordination, as shown in Fig. 1(c). The remaining four copper atoms in the unit cell are in nearly linear coordination, with Cu-S distances of about 2.3 Å but with a third sulfur atom at a distance >3.0 Å towards a distorted trigonal planar coordination.

At pressures above ~3 GPa the reflections of the copper sulfide samples were indexed with a smaller monoclinic unit cell with $a = 10.312(4)$ Å, $b = 6.737(3)$ Å, $c = 7.305(1)$ Å, and $\beta = 100.17(2)^\circ$ [6.2(3) GPa]. The structure of this first high-pressure polymorph of α-chalcocite, HP1, was first solved at different pressures [4.6(2) and 6.2(3) GPa] in the noncentrosymmetric space group $P2_1$ with 14 Wyckoff positions for copper (2a) and 6 for sulfur (2a). After the first refinements of the atomic positions and the anisotropic displacement parameters, two copper positions showed unusually high values for the displacement parameters in one direction and were therefore split into four positions with refined site occupation factors of nearly 0.5. The program PLATON [35] was used to search for any missed symmetry. The program suggested a model based on space group $P2_1/c$, including two split positions for copper with a site occupation factor of 0.5, resulting in a structural model similar to that before with space group $P2_1$. Looking at the systematic extinction, no reflection violates the extinction rules of space group $P2_1$. However, as only one unique reflection out of 1754 violates the extinction rules of $P2_1/c$, we have chosen the structural model based on space group $P2_1/c$. The atomic positions and anisotropic displacement parameters for this model were refined successfully at different pressures (Table I and Supplemental Material [21]). The structure is based on a distorted hexagonal close packing of sulfur as shown in Fig. 4(a) with seven Wyckoff positions (4e) for copper and three positions (4e) for sulfur with structural properties

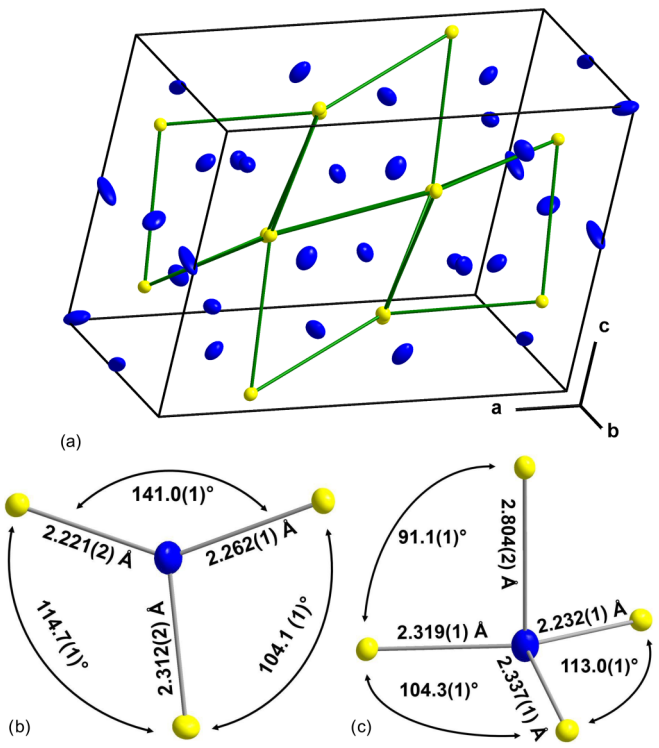

FIG. 4. Structural properties of the first high-pressure polymorph of α-chalcocite, HP1, at 6.2(3) GPa evaluated by single-crystal x-ray diffraction [$a = 10.312(4)$ Å, $b = 6.737(3)$ Å, $c = 7.305(1)$ Å, and $\beta = 100.17(2)^\circ$]. (a) Unit cell of HP1. Blue: copper; yellow: sulfur; green lines: indication of the distorted hexagonal close packing of sulfur. (b) Trigonal planar coordination of copper in HP1: typical values for Cu-S distances and angles. (c) Fourfold coordination of copper in HP1 showing a distorted tetrahedral character: typical values for Cu-S distances and angles.

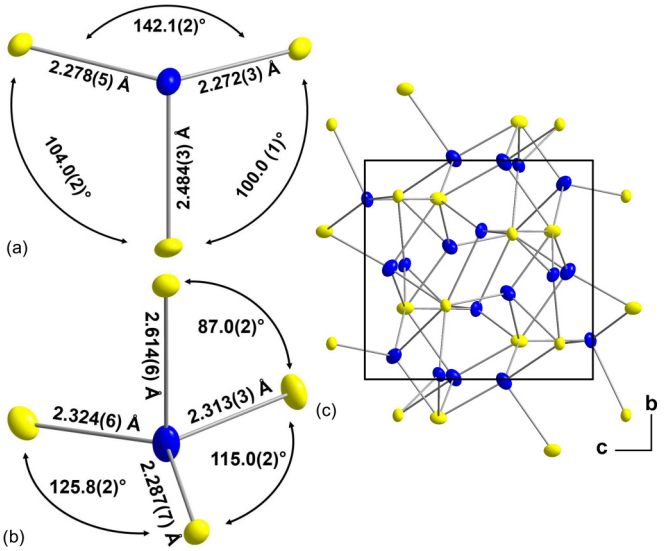

FIG. 5. Structural properties of the second high-pressure phase of α-chalcocite, HP2, at 9.6(5) GPa evaluated by single-crystal x-ray diffraction [$a = 6.7127(6)$ Å, $b = 6.6764(8)$ Å, $c = 6.9661(9)$ Å, and $\beta = 93.17(2)^\circ$]. (a) Trigonal planar coordination of copper in HP2. (b) Fourfold coordination of copper in HP2 showing a distorted tetrahedral character: typical values for Cu-S distances and angles. (c) View along the crystallographic axis a. Blue: copper; yellow: sulfur.

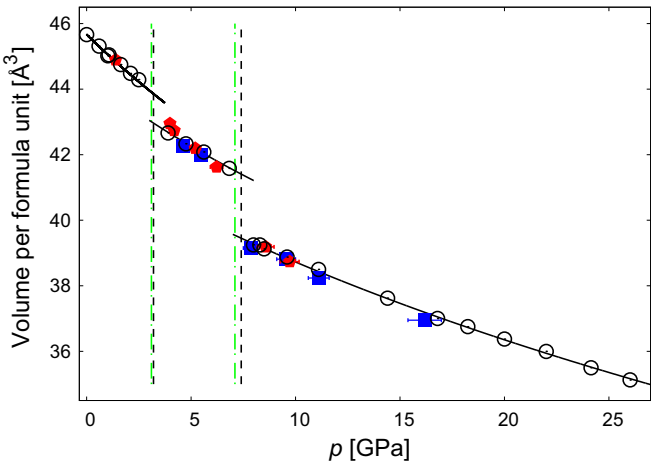

FIG. 6. Volume per formula unit of Cu_2S as a function of pressure up to 26 GPa. Red pentagons: single-crystal x-ray diffraction data using a mixture of methanol and ethanol (4:1) as the pressure-transmitting medium; blue squares: single-crystal x-ray diffraction data using neon as the pressure-transmitting medium; black circles: data points published by Santamaría-Pérez *et al.* [20]; black lines: equations of state for the ambient phase and the high-pressure phases, HP1 and HP2, published by Santamaría-Pérez *et al.* [20]; green dot-dashed lines: transition pressures evaluated by high-pressure single-crystal x-ray diffraction experiments; black dashed lines: transition pressures evaluated by Santamaría-Pérez *et al.* [20] using powder x-ray diffraction.

similar to those of α-chalcocite. In one unit cell 14 of the 24 copper atoms are coordinated trigonal planar, as pictured in Fig. 4(b). Eight copper atoms are coordinated by four sulfur atoms forming a distorted tetrahedral environment [Fig. 4(c)]. With copper-copper and sulfur-sulfur distances larger than 2.5 and 3 Å, respectively, the structure fits well into the scheme of copper sulfide structures [1,15,36,37].

At 7.9(4) GPa the reflections of the samples were indexed with yet another monoclinic unit cell with $a = 6.7313(5)$ Å, $b = 6.6978(6)$ Å, $c = 6.958(6)$ Å, and $\beta = 93.08(2)^\circ$, indicating that a structural phase transition from monoclinic HP1 to monoclinic HP2 takes place between 6.2(3) and 7.9(4) GPa. The structure was solved at different pressures [7.9(4), 9.6(5), 11(1), 16(1) GPa] in space group $P2_1/c$ with four Wyckoff positions for copper (4e) and two for sulfur (4e). The atomic positions and thermal displacement parameters were refined successfully (Table I and Supplemental Material [21]). As shown in Fig. 5 in one unit cell four copper atoms are coordinated trigonal planar by sulfur, four copper atoms are fourfold coordinated towards a distorted tetrahedral environment, and eight copper atoms are in a distorted tetrahedral coordination with a fifth sulfur atom at a distance longer than 3 Å towards a strongly distorted fivefold coordination. The copper-copper distances and the sulfur-sulfur distances are larger than 2.5 and 3 Å, respectively, similar to the distances in other copper sulfide structures [1,15,36,37] and in agreement with the polymorphs at lower pressure.

The lattice parameters of our structural models for the two high-pressure polymorphs (HP1, HP2) of monoclinic α-chalcocite are in good agreement with the lattice parameters Santamaría-Pérez *et al.* [20] derived from tentative indexations of powder x-ray diffraction data (see the Supplemental Material [21] for a direct comparison). In Fig. 6 the volume per formula unit of Cu_2S is given as a function of pressure based on the data from the present work and the data from Santamaría-Pérez *et al.* [20]. A similar behavior of the pressure dependence of the volume is observed in the present study and in the work by Santamaría-Pérez *et al.* [20], showing a larger volume collapse across the second pressure-induced phase transition around 7 GPa (∼5%) in comparison to the collapse across the first transition at around 3 GPa (∼3%). The volume collapses across the transitions indicate that both phase transitions are of first order.

B. Structural relations

In all three polymorphs (α-chalcocite, HP1, HP2) the sulfur-sulfur and copper-copper distances are larger than 3.5 and 2.5 Å, respectively. This is a general feature of copper sulfides at ambient pressures [1,15,36,37] which seems to be valid for elevated pressures as well. The copper-sulfur distances for the trigonal planar coordination and the distorted tetrahedral coordination are displayed as a function of pressure in Figs. 7(a) and 7(b), respectively.

At ambient conditions the structure of α-chalcocite, Cu_2S, is based on a hexagonal close packing of sulfur. Within this sulfur sublattice most of the copper atoms are coordinated by three sulfur atoms in a slightly distorted trigonal planar environment with copper-sulfur distances between 2.2 and 2.4 Å [Fig. 7(a)]. Some of these copper atoms are coordinated by a fourth sulfur atom at a distance between 2.8 and 3.4 Å, forming a strongly distorted tetrahedral coordination [Fig. 7(b)]. These structural

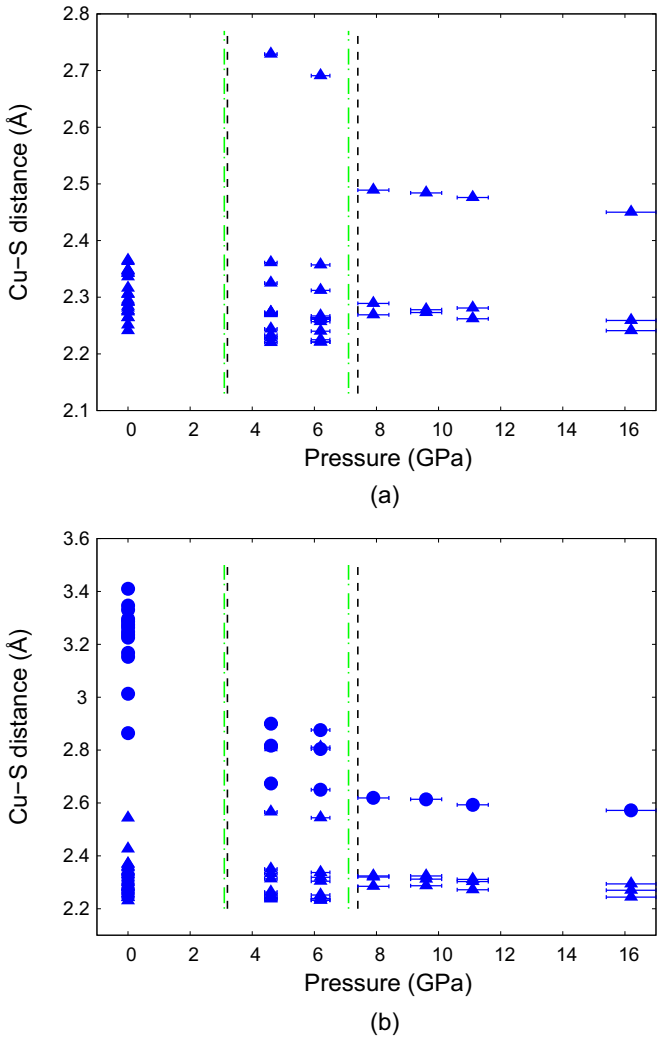

FIG. 7. Copper-sulfur distances as a function of pressure for (a) copper in the trigonal planar coordination and (b) copper in fourfold coordination. Blue triangles: copper-sulfur distances for the trigonal planar environment; blue dots: copper-sulfur distances between the copper atom in trigonal coordination and the fourth sulfur atom towards a distorted tetrahedral environment; green dot-dashed lines: transition pressures evaluated by high-pressure single-crystal x-ray diffraction experiments; black dashed lines: transition pressures evaluated by Santamaría-Pérez *et al.* [20] using powder x-ray diffraction.

features are also found in the first high-pressure polymorph, HP1. On an increase in pressure, the fourth sulfur atom moves closer to the planar coordinated copper, thus reducing the distortion of the distorted tetrahedral environment. In addition, a distorted planar coordination of copper is present with two nearly equidistant copper-sulfur distances of about 2.3 Å and a third sulfur in an elongated distance of about 2.7 Å. In comparison to the polymorphs at lower pressure the structure of HP2 is not based on a hexagonal close packing of sulfur. Furthermore, the distorted fourfold coordination of copper replaces the trigonal planar coordination as the dominant coordination in the structure, with an additional trend towards strongly distorted five- and sixfold coordinations.

The crystal structure of α-chalcocite can be described using a simplified model in which only the sheets of sulfur atoms

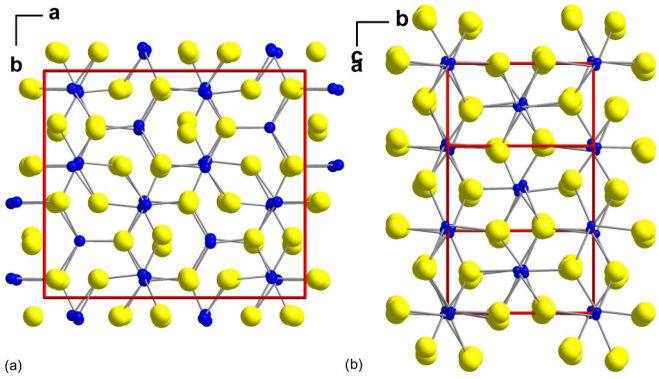

FIG. 8. Simplified structural models of (a) α-chalcocite and (b) HP1 accounting for only the copper atoms within the sulfur layers of the distorted hexagonal close packing. The view is orthogonal to the sulfur layers.

forming a distorted hexagonal close packing with copper in threefold coordination within these layers are considered. In Fig. 8(a) such a simplified model is shown with the viewing direction orthogonal to the layers of sulfur. The crystal structure of HP1 is also based on a hexagonal close packing of sulfur, and it is possible to describe it in the same simplified way as the structure of α-chalcocite. In a first approximation the simplified model of the structure of HP1 is related to the simplified model of α-chalcocite by a rotation of about 43° around the b axis, as pictured in Fig. 8(b).

C. Electrical resistance

The pressure dependence of the electrical resistance of α-chalcocite under compression is shown in Fig. 9. The resistance of α-chalcocite is independent of pressure and does not change significantly up to a pressure of about 3 GPa, where the

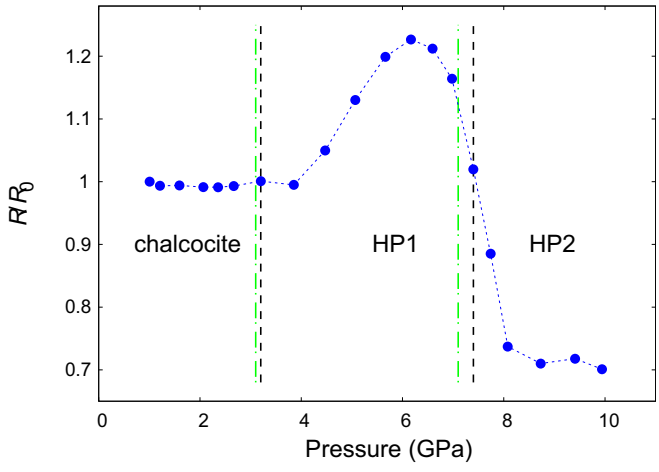

FIG. 9. Changes of the electrical resistance of Cu_2S as a function of pressure using a mixture of Al_2O_3 and epoxy resin as the pressure-transmitting medium in a diamond-anvil cell. Blue dots: measured data (error bars are smaller than symbol size); green dot-dashed lines: transition pressures evaluated by high-pressure single-crystal x-ray diffraction experiments; black dashed lines: transition pressures evaluated by Santamaría-Pérez *et al.* [20] using powder x-ray diffraction.

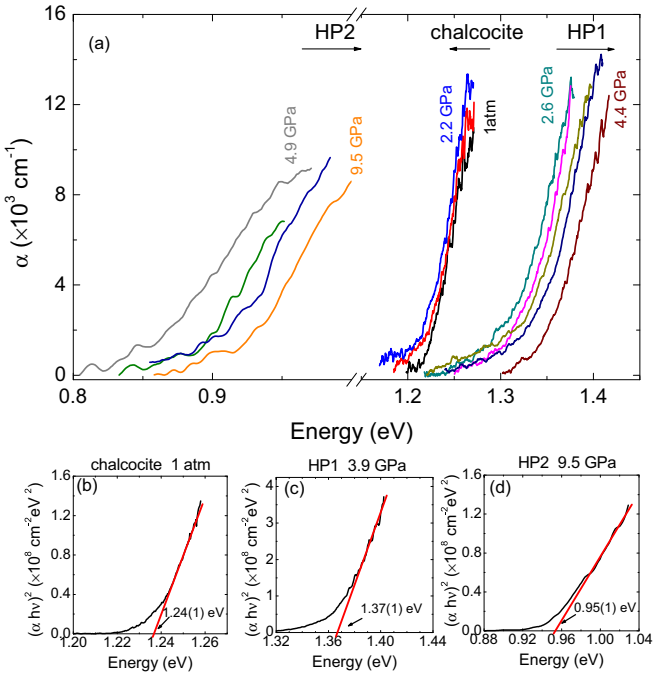

FIG. 10. (a) Absorption spectra of Cu_2S at different pressures on pressure release from 9.5 GPa to ambient pressure. The energy dependence of $(h\nu\alpha)^2$ and the extrapolation of the linear portion intercepting the energy axis are shown for (b) α-chalcocite at 1 atm, (c) HP1 at 3.9(2) GPa, and (d) HP2 at 9.5(5) GPa.

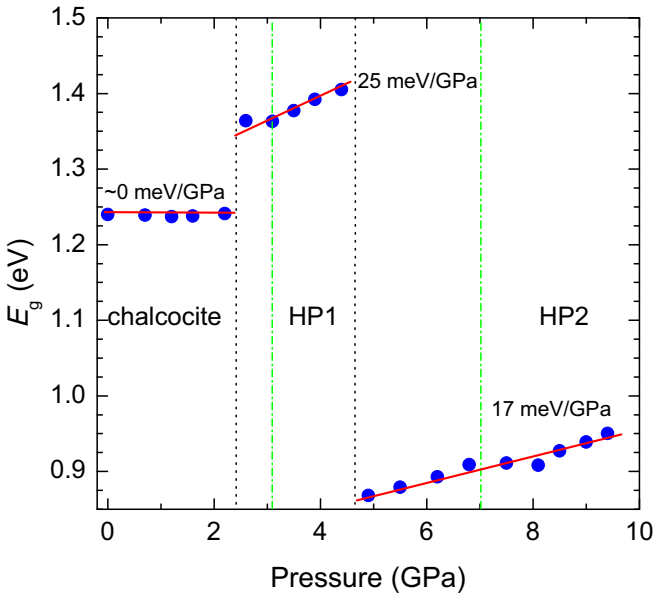

FIG. 11. Pressure dependence of the band gap E_g on pressure release. Blue dots: values extracted from the analysis of the spectra shown in Fig. 10; red solid lines: linear fits to the data; black dashed lines: transition pressures obtained in the optical absorption experiment on pressure release; green dot-dashed lines: transition pressures evaluated by high-pressure single-crystal x-ray diffraction experiments on pressure increase.

first pressure-induced structural phase transition takes place according to our high-pressure single-crystal x-ray diffraction experiments. Above 3 GPa the electrical resistance gradually increases as a function of pressure. At pressures around 7 GPa, where the second pressure-induced structural phase transition occurs, a sudden drop in the electrical resistance is observed, with a subsequent stabilization upon further compression up to ∼10 GPa.

Considering that Cu_2S shows p-type conduction, the pressure-induced increase in the resistance in HP1 and the drop observed during the formation of HP2 indicate that the structural phase transitions also involve changes at the top of the valence band of the different polymorphs that might influence the optical properties of the different polymorphs of Cu_2S.

D. Optical absorption

Figure 10(a) shows selected absorption spectra at high pressure of Cu_2S. The data collection was performed on pressure release with the same sample and loading employed to carry out the single-crystal x-ray diffraction experiment in which a mixture of methanol and ethanol was used. Therefore, our starting pressure was 9.5(5) GPa.

As pressure decreases from 9.5(5) GPa, the absorption edge shifts to lower energies while keeping the same shape up to 4.9(2) GPa, when it abruptly widens around 0.45 eV, changing its shape. This abrupt change at ∼4.7 GPa, related to an increase in the band gap, is observed 2.5 GPa below the HP1 to HP2 phase transition as a result of the hysteresis shown by this first-order phase transition. In HP1 the band gap decreases with decreasing pressure up to 2.2(1) GPa, when the absorption edge drops again, changing its shape. This second abrupt change is related to the HP1 to α-chalcocite back transformation and is observed on pressure release at a pressure 0.5 GPa below the value obtained on pressure increase. This indicates its first-order character. In this case the phase transition also involves a volume change which, however, is much smaller than in the HP1 to HP2 phase transition (Fig. 6). Below 2.4 GPa the absorption edge is almost pressure independent.

In order to determine the nature of the transition of the band gap of each phase we plotted the absorption coefficient of each phase either as $(h\nu\alpha)^2$ (direct) or $(h\nu\alpha)^{1/2}$ (indirect) as a function of energy [38,39] and selected from both plots the one with a longer linear range. The best fits are shown in Figs. 10(b), 10(c) and 10(d). We found a direct band gap for α-chalcocite, HP1, and HP2. After this analysis the value of the band gap E_g was obtained from each spectrum as the intercept of the high-energy linear part of $(h\nu\alpha)^2$ with the energy axis. We also plotted $\ln(\alpha)$ as a function of energy for the three phases, observing that different from the tetragonal [13] polymorph of Cu_2S, in our case the absorption edge cannot be explained with an Urbach tail [40].

The pressure dependence of the band gap E_g is shown in Fig. 11. The behavior of the absorption edge shown in Fig. 10 is reflected in the determined band gap E_g obtained according to the analysis explained above for each phase as illustrated in Figs. 10(b), 10(c) and 10(d). E_g is pressure independent in the α-chalcocite phase up to 2.2(1) GPa, when the phase transition occurs, with E_g widening from 1.24 to 1.35 eV in HP1. E_g shifts at 25 meV/GPa in HP1 up to 4.4(2) GPa, when it collapses from 1.41 to 0.87 eV at 4.9(2) GPa because of the

TABLE II. Lattice parameters of the three polymorphs ($P2_1/c$) of Cu_2S from single-crystal x-ray diffraction (exp.) and DFT-based calculations (calc.).

	p (GPa)	a (Å)	b (Å)	c (Å)	β (°)	V (Å^3)
α-chalcocite (exp.)	0.0001	15.1882(6)	11.8511(4)	13.465(5)	116.263(8)	2173.5(1)
α-chalcocite (calc.)	0	15.233	11.962	13.438	116.22	2196.8
HP1 (exp.)	6.2(3)	10.312(4)	6.737(3)	7.305(1)	100.17(2)	499.5(1)
HP1 (calc.)	6.2	10.3350	6.8039	7.3048	100.79	504.6
HP2 (exp.)	8.6(5)	6.712(4)	6.6905(6)	6.977(2)	93.27(5)	312.7(2)
HP2 (calc.)	8.6	6.6946	6.664	7.0217	93.83	312.56

structural transition of HP1 to HP2. In HP2 E_g increases at 17 meV/GPa.

E. Calculations

In Table II the lattice parameters of the three polymorphs of Cu_2S (α-chalcocite, HP1, HP2) derived from single-crystal diffraction experiments are given in comparison to the values obtained from our DFT-based calculations. For all three polymorphs the deviation of the calculated lattice parameters from the experimental values is $\leqslant 1\%$, indicating that our calculations model the three polymorphs well.

The calculated band structures of the three polymorphs are presented in Fig. 12. As observed in other phases of Cu_2S [13] or Cu_2O [41] and in the three electronic band structures shown in Fig. 12, in this compound the top of the valence band has a marked Cu d character, while the lowest part of the conduction band is mainly contributed by the Cu s orbitals. Hence, the top of the valence band shows low dispersion, while the bottom of the conduction band, with the d electrons having a larger effective mass m_v^* than the s electrons, is characterized by a large dispersion. A close inspection of the electronic band structures shows that the band gaps of the α-chalcocite and the HP2 phases are direct at Γ, and the band gap of HP1 is indirect. In particular, the indirect band gap of HP1 occurs between the B and the Γ points of the Brillouin zone. However, in HP1 the difference between the indirect $B\Gamma$ transition and the direct one at Γ is only 0.05 eV, and therefore, most likely, that is the transition that we are experimentally observing. Regarding the calculated values of the band gaps, in the case of α-chalcocite, the calculated value is 0.3 eV at ambient pressure, 0.9 eV below the observed experimental value. Considering that DFT calculations generally underestimate the band gap and that the ground states are accurately determined in our calculations, we assume such an underestimation also for HP1 and HP2. This assumption would provide calculated values of 1.5 eV at 6.2 GPa and 0.92 eV at 8.6 GPa, in good agreement with the obtained experimental values.

Another conclusion that can be drawn from the calculated electronic band structures is related to the observed pressure dependence of the resistance shown in Fig. 9. From our resistance measurements no information can be obtained on the density of holes or their mobility in the three polymorphs. However, we can infer some information from the calculated top of the valence bands. In intrinsic semiconductors such as ours conductivity occurs due to hydrogenic impurities. Thus, since Cu_2S is a p-type semiconductor and considering the $k \cdot p$ model and a parabolic valence band at the top of the valence band at Γ, the mobility of the holes depends on the effective mass m_h^*, which increases with a decrease in the band dispersion. Therefore, a possible explanation for the increase in the resistance in HP1 compared to α-chalcocite might be a decrease in the dispersion of the top of the valence band. With respect to the decrease in resistance in the HP2 phase, apart from considering the abrupt collapse of 0.45 eV suffered by the band gap, which indicates a tendency to metalization, we also observe a change at the top of the valence band. Whereas the top of the valence band of α-chalcocite and HP1 are not degenerated at Γ, in the case of HP2 the uppermost part of the valence band at Γ is doubly degenerated. This double degeneration necessarily implies an increase in the density of states. Since the number of holes at the top of the valence band

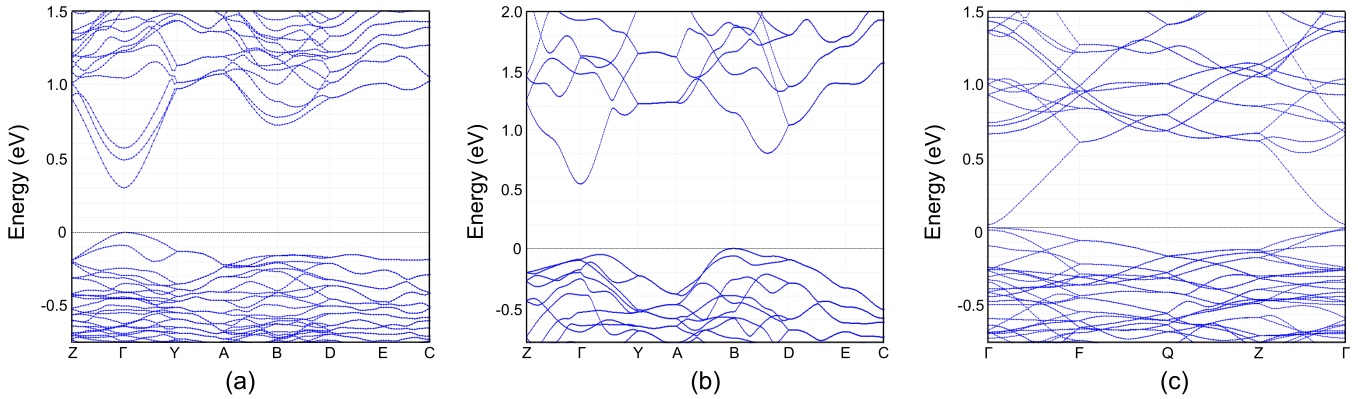

FIG. 12. Electronic band structure of the (a) ambient pressure phase of α-chalcocite, (b) its first high-pressure phase (HP1; 6.2 GPa), and (c) its second high-pressure phase (HP2; 8.6 GPa) from the DFT-based calculations.

P_h^v is proportional to the density of states [42], the resistivity and therefore the resistance of HP2 drastically reduce with respect to those of α-chalcocite and HP1.

V. CONCLUSIONS

In this study we have investigated the high-pressure behavior of monoclinic α-chalcocite, Cu_2S, using single-crystal x-ray diffraction, electrical resistance measurements, and optical absorption spectroscopy. Previous studies on α-chalcocite have shown that at ambient temperature this compound undergoes two pressure-induced structural phase transitions at 2.4 and 4.4 GPa, according to Wang *et al.* [19], and at 3.2 and 7.4 GPa, according to Santamaría-Pérez *et al.* [20]. The transition pressures derived from the experimental results of the present study (x-ray diffraction on compression: ∼3.1 and ∼7.1 GPa; optical absorption on decompression: ∼2.2 and ∼4.7 GPa) are slightly different from the pressures obtained in the earlier studies, which might arise from different grain sizes of the samples, different pressure-transmitting media, different experimental techniques, and the hysteresis upon compression and decompression. Wang *et al.* [19] and Santamaría-Pérez *et al.* [20] derived different unit-cell parameters for the two high-pressure polymorphs (HP1 and HP2) of monoclinic α-chalcocite. Our solutions and refinements of the crystal structures of HP1 and HP2 at different pressures agree with the cells proposed by Santamaría-Pérez *et al.* [20] (see the Supplemental Material [21] for a brief comparison between the lattice parameters from previous works and the present study). HP1 crystallizes in space group $P2_1/c$ with $a = 10.312(4)$ Å, $b = 6.737(3)$ Å, $c = 7.305(1)$ Å, and $\beta = 100.17(2)^\circ$ at 6.2(3) GPa, and HP2 crystallizes in space group $P2_1/c$ with $a = 6.731(4)$ Å, $b = 6.689(2)$ Å, $c = 6.967(8)$ Å, and $\beta = 93.18(3)^\circ$ at 7.9(4) GPa. Solving the crystal structures of the high-pressure polymorphs of α-chalcocite, HP1 and HP2, has allowed us to perform calculations of their electronic band structures on the basis of which we have been able to interpret our resistance and optical absorption edge experiments. We have found that all the polymorphs present a direct band gap at zone center Γ which is pressure independent in the α-chalcocite phase and increases under compression at 25 and 17 meV/GPa for HP1 and HP2, respectively. The collapse of the band gap of 0.45 eV observed in the HP1 to HP2 phase transition is concomitant with a resistance drop of 42% interpreted as being due to an increase in the number of holes P_h^v at the uppermost part of the valence band as a result of a double degeneration of the band in HP2.

Based on the work by Ruehle [43] the theoretical maximum of the conversion efficiency of a single-junction solar cell (Shockley-Queisser limit [44]) under standard solar-cell test conditions is obtained for a band gap of ∼1.4 eV. Our study shows that the band gap of α-chalcocite (∼1.2 eV at ambient conditions) can be tuned towards a value of ∼1.4 eV by a pressure-induced phase transition around 3 GPa.

ACKNOWLEDGMENTS

Financial support from the Goethe-University Frankfurt am Main, the DFG (Wi 1232), and the BMBF (05K16RFA, 05K16RFB) is gratefully acknowledged. J.R.-F. and D.S.-P. acknowledge the Spanish Ministry of Economy and Competitiveness (MINECO) for the Juan de la Cierva (IJCI-2014-20513) and Ramón y Cajal (RYC-2014-15643) programs, respectively. MINECO is also acknowledged for financial support from Projects No. MAT2016-75586-C4-1/3-P and No. MAT2015-71070-REDC (MALTA Consolider). A.F. thanks the Julius-Maximilians-Universität Würzburg for financial support. We acknowledge Prof. J. González from the Universidad de Cantabria for fruitful discussions. D.Z. acknowledges C. Neun for support with sample preparation. Parts of the research were carried out at the light source PETRA III at DESY, a member of the Helmholtz Association (HGF). We would like to thank H.-P. Liermann and his team for assistance in using beamline P02.2.

[1] H. T. J. Evans, Nat. Phys. Sci. **232**, 69 (1971).
[2] E. Hirahara, J. Phys. Soc. Jpn. **6**, 422 (1951).
[3] T. Miller, J. Wittenberg, H. Wen, S. Connor, Y. Cui, and A. Lindenberg, Nat. Commun. **4**, 1369 (2013).
[4] R. Marshall and S. S. Mitra, J. Appl. Phys. **36**, 3882 (1965).
[5] B. Selle and J. Maege, Phys. Status Solidi **30**, K153 (1968).
[6] N. Nakayama, Jpn. J. Appl. Phys. **8**, 450 (1969).
[7] A. Rothwarf, Solar Cells **2**, 115 (1980).
[8] A. Putnis, Philos. Mag. **34**, 1083 (1976).
[9] K. L. Chopra and S. R. Das, *Thin Film Solar Cells* (Plenum, New York, 1983).
[10] W. van der Stam, A. C. Berends, and C. de Mello Donega, ChemPhysChem **17**, 559 (2016).
[11] A. Janosi, Acta Crystallogr. **17**, 311 (1964).
[12] T. Machani, D. P. Rossi, B. J. Golden, E. C. Jones, M. Lotfipour, and K. E. Plass, Chem. Mater. **23**, 5491 (2011).
[13] D. Zimmer, J. Ruiz-Fuertes, L. Bayarjargal, E. Haussühl, B. Winkler, J. Zhang, C. Q. Jin, V. Milman, E. Alig, and L. Fink, Phys. Rev. B **96**, 054108 (2017).
[14] M. J. Buerger and N. W. Buerger, Am. Mineral. **29**, 55 (1944).
[15] H. T. J. Evans, Z. Kristallogr. **150**, 299 (1979).
[16] B. J. Skinner, Econ. Geol. **65**, 724 (1970).
[17] K.-F. Seifert, Fortschr. Mineral. **45**, 214 (1968).
[18] E. Hinze and A. Neuhaus, Naturwissenschaften **56**, 136 (1969).
[19] S. Wang, L. Guo, X. Wen, S. Yang, J. Zhao, J. Liu, and Z. Wu, Mater. Chem. Phys. **75**, 32 (2002).
[20] D. Santamaría-Pérez, G. Garbarino, R. Chuliá-Jordan, M. A. Dobrowolski, C. Mühle, and M. Jansen, J. Alloys Compd. **610**, 645 (2014).
[21] See Supplemental Material at http://link.aps.org/supplemental/10.1103/PhysRevB.97.134111 for crystallographic data, CIF files, the results of the energy-dispersive x-ray spectroscopy analysis, and further details.
[22] H. Rietveld, J. Appl. Crystallogr. **2**, 65 (1969).
[23] A. C. Larson and R. B. Von Dreele, General Structure Analysis System (GSAS), Los Alamos National Laboratory Report LAUR 86-748 (2000), https://www.ncnr.nist.gov/xtal/software/gsas.html.
[24] B. H. Toby, J. Appl. Crystallogr. **34**, 210 (2001).
[25] R. Boehler, Rev. Sci. Instrum. **77**, 115103 (2006).

[26] H. K. Mao, J.-A. Xu, and P. M. Bell, J. Geophys. Res. **91**, 4673 (1986).
[27] H.-P. Liermann, Z. Konopkova, W. Morgenroth, K. Glazyrin, J. Bednarcik, E. E. McBride, S. Petitgirard, J. T. Delitz, M. Wendt, Y. Bican *et al.*, J. Synchrotron Radiat. **22**, 908 (2015).
[28] Agilent, CRYSALIS^{PRO} software system, version 1.171.36.28, Agilent Technologies UK Ltd., Oxford, 2013.
[29] L. Palatinus and G. Chapuis, J. Appl. Crystallogr. **40**, 786 (2007).
[30] V. Petricek, M. Dusek, and L. Palatinus, Z. Kristallogr. **229**, 345 (2014).
[31] P. Hohenberg and W. Kohn, Phys. Rev. **136**, B864 (1964).
[32] J. P. Perdew, K. Burke, and M. Ernzerhof, Phys. Rev. Lett. **77**, 3865 (1996).
[33] S. J. Clark, M. D. Segall, C. J. Pickard, P. J. Hasnip, M. I. J. Probert, K. Refson, and M. C. Payne, Z. Kristallogr. **220**, 567 (2005).
[34] H. J. Monkhorst and J. D. Pack, Phys. Rev. B **13**, 5188 (1976).
[35] A. L. Spek, Acta Crystallogr. D **65**, 148 (2009).
[36] H. T. J. Evans, Am. Mineral. **66**, 807 (1981).
[37] N. Morimoto, K. Koto, and Y. Shimazaki, Am. Mineral. **54**, 1256 (1969).
[38] J. Tauc, Mater. Res. Bull. **3**, 37 (1968).
[39] E. A. Davis and N. F. Mott, Philos. Mag. A **22**, 903 (1970).
[40] F. Urbach, Phys. Rev. **92**, 1324 (1953).
[41] P. Lukashev, W. R. L. Lambrecht, T. Kotani, and M. van Schilfgaarde, Phys. Rev. B **76**, 195202 (2007).
[42] N. Ashcroft and N. Mermin, *Solid State Physics* (Saunders College, Philadelphia, 1976).
[43] S. Ruehle, Sol. Energy **130**, 139 (2016).
[44] W. Shockley and H. J. Queisser, J. Appl. Phys. **32**, 510 (1961).